Letter | Editors' Suggestion | Featured in Physics

Capillary surfers: Wave-driven particles at a vibrating fluid interface

Ian Ho,[1,*] Giuseppe Pucci,[1,2,*] Anand U. Oza,[3] and Daniel M. Harris[1,†]
[1]*School of Engineering, Brown University, Providence, Rhode Island 02912, USA*
[2]*University of Rennes, CNRS, IPR (Institut de Physique de Rennes), UMR 6251, F-35000 Rennes, France*
[3]*Department of Mathematical Sciences & Center for Applied Mathematics and Statistics, New Jersey Institute of Technology, Newark, New Jersey 07102, USA*

(Received 8 April 2021; accepted 15 August 2023; published 7 November 2023)

We present an experimental study of capillary surfers, a new fluid-mediated active system that bridges the gap between dissipation- and inertia-dominated regimes. Surfers are wave-driven particles that self-propel and interact on a fluid interface via an extended field of surface waves. A surfer's speed and interaction with its environment can be tuned broadly through the particle, fluid, and vibration parameters. The wave nature of interactions among surfers allows for multistability of interaction modes and promises a number of novel collective behaviors.

DOI: 10.1103/PhysRevFluids.8.L112001

Active matter systems have recently attracted considerable interest for the possibility of extending statistical mechanics to incorporate nonequilibrium phenomena, as their constituents locally consume energy in order to move or exert forces on each other [1,2]. There has been extensive work on dissipation- [3–16] and inertia-dominated [17–23] active systems (e.g., bacterial suspensions and fish schools, respectively), but our understanding of the intermediate regime [24] between these two extremes is currently limited [25]. Self-propelled particles are natural or artificial particles that generally represent the constituents of such active systems, as they convert energy from the environment into directed motion [26].

Vibrating platforms are suitable sources of diffuse energy to observe macroscopic self-propelled particles [27,28] and their collective behavior [29–34]. Indeed, solid asymmetric particles can self-propel with an internal source of energy [35,36] or by rectifying the mechanical vibrations of the platform on which they move [27,37,38]. In particular, such "dry" active systems [39] represent important and successful platforms to demonstrate collective behavior in table-top experiments and to evaluate theoretical predictions. On the other hand, fluid interfaces are convenient platforms for the self-propulsion of natural [40] and artificial bodies, including solid particles [41–45], drops [28,46–48], and small-scale robots [49]. When the fluid interface is vibrating, millimetric droplets may self-propel by bouncing on the sloped surface wave they generate in select parameter regimes [28,50], and floating drops may be deformed and driven by surface waves [46–48]. For floating drops, propulsion mechanisms based on asymmetric vortex generation [48] and wave radiation pressure [47] have been proposed, but the drops are difficult to manipulate directly due to their self-adaptive nature. The study of capillary wave-driven bodies at the fluid interface is relevant to the propulsion of [40,51,52] and interactions between [53,54] water-walking insects, controlled particle transport and patterning at fluid interfaces [55–57], and novel propulsion mechanisms for autonomous interfacial "micro"-robots [43,58].

We here introduce capillary surfers [Fig. 1(a)]: highly tunable solid particles that self-propel on a vibrating liquid surface due to the asymmetric radiation pressure of their self-generated surface

*Co-first author.
†Corresponding author: daniel_harris3@brown.edu

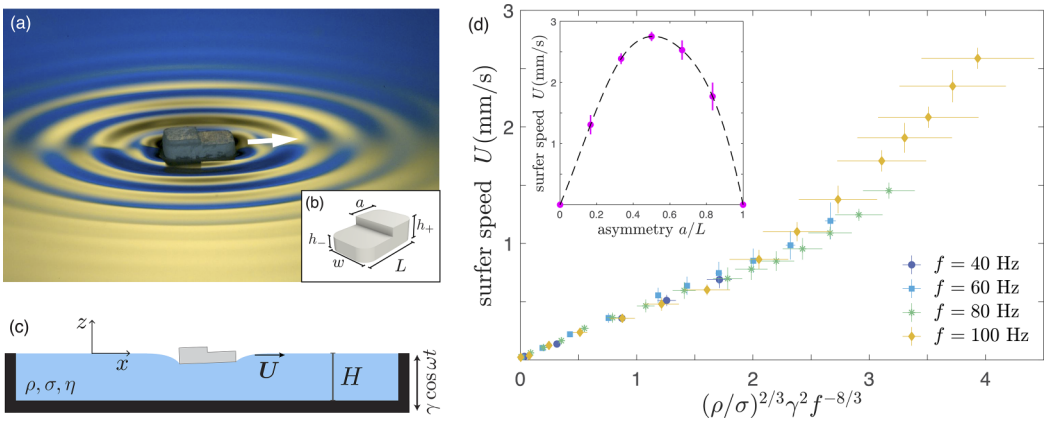

FIG. 1. A capillary surfer self-propels on a fluid interface due to its self-generated waves (supplementary video 1). (a) Oblique wave field visualization, in which colors are obtained from the distorted reflection of a yellow and blue background on the fluid surface. (b) Surfer geometry. (c) Side view schematic of the experimental setup (not to scale). The fluid has density ρ, surface tension σ, dynamic viscosity η, and depth H. (d) Dependence of the surfer speed U on the forcing frequency f and forcing acceleration γ, as collapsed by the nondimensional propulsive force scaling in Eq. (1), with $L = 4.20 \pm 0.03$ mm, $w = 2.70 \pm 0.03$ mm, $a = L/2$. Inset: Dependence of U on the asymmetry a/L for $f = 100$ Hz, $\gamma = 3.3$ g, $L = 6.44 \pm 0.02$ mm, $w = 4.13 \pm 0.02$ mm.

waves. Two surfers interact via these surface waves and self-organize into multiple interaction modes, while multiple surfers exhibit collective behaviors. Generally, our results suggest that capillary surfers hold promise as a platform that bridges the gap between dissipation- and inertia-dominated active systems.

Millimetric surfers [Fig. 1(b)] with width $w = 1.75$–7.09 mm and length $L = 2.78$–10.85 mm were manufactured out of white polytetrafluoroethylene (PTFE) sheets with density 2.2 g/cm^3, which are chemically hydrophobic. An adhesive PTFE sheet with thickness 0.40 mm was attached to the upper surface of a PTFE sheet with thickness 0.82 mm. A laser cutter (Universal Laser Systems, VLS 4.60) was then used to cut out rectangular profiles with rounded corners (with radius equal to $0.17L$) to avoid sharp corners along the contact line, which were observed to reduce the reproducibility of the surfer motion due to irregular wetting. In order to introduce an asymmetry in the surfer distribution of mass, a laser engraved line was used as a guide to cut out a portion of the upper adhered layer using a fine razor. Taking inspiration from marine terminology, in the following we refer to the front and back of the surfer as the "bow" and "stern," respectively. The height of the surfer's stern and bow were $h_+ = 1.22$ mm and $h_- = 0.82$ mm, respectively. The center of mass of the surfers was thus offset with respect to their in-plane geometric center. Surfers were gently deposited on a bath of water-glycerol mixture with density $\rho = 1.1756 \pm 0.0003$ g/cm^3, viscosity $\eta = 0.0197 \pm 0.0005$ Pa s, surface tension $\sigma = 66.4 \pm 0.5$ mN/m, and depth $H = 5.73 \pm 0.06$ mm and supported at the liquid-air interface by virtue of the equilibrium between their weight, hydrostatic forces, and surface tension. The contact line of the bath was pinned to the surfer's base perimeter. As a result of their mass asymmetry, surfers were slightly tilted in equilibrium [Fig. 1(c)] and the deformation of the interface varied along their perimeter. For the parameters explored here, the surfer's tilt during oscillation was substantially smaller than the tilt of asymmetric self-propelled granular particles on a vibrating plate [27]. With a pinned contact line and symmetric contact area, mass asymmetry was a requirement to obtain self-propulsion, yet propulsion can be realized with virtually any surfer shape. The liquid bath was vertically driven by an electromagnetic shaker with acceleration $\Gamma(t) = \gamma \cos(2\pi f t)$ with f the forcing frequency in the range 40–100 Hz. All experiments were performed below the Faraday threshold, the critical vibration amplitude above

which subharmonic standing waves form spontaneously at the free surface [59]. A viscous mixture of water and glycerol was used to increase the Faraday threshold, thereby expanding the accessible driving parameter regime for the present study. Steady and unsteady Faraday wave fields have been previously shown to result in passive particle migration [45] and redistribution [56,60]. A monochrome USB camera (Allied Vision, Mako) with a macro lens for video acquisition was mounted above the bath and normal to its surface. In order to increase the contrast of the video recordings, the bath's base was constructed of a black acrylic plate. The shaker system was placed inside an acrylic box to isolate the bath from ambient air currents and contaminants. More details on experimental methods and procedures are available in Supplemental Material [61].

As soon as the bath was set into vibration, a surfer generated propagating surface waves as a result of the relative vertical motion between the surfer and bath, a consequence of the difference in inertia between the surfer and the liquid. Correspondingly, the surfer moved along its long axis in the direction of its thinner half [Figs. 1(a) and 1(c)]. The contact line remained pinned to the surfer's base perimeter at all times. Due to the frequencies considered, surface waves were in the capillary regime with wavelength $\lambda = 2\pi/k$ given by the dispersion relation $(2\pi f)^2 = \sigma k^3/\rho$ in the deep-water limit $kH \gg 1$. In the parameter regime explored, $\lambda = 3.3$–5.2 mm, which is comparable to the surfer size. In the absence of external perturbations or manufacturing imperfections, the surfer moved with constant velocity $\boldsymbol{U}$ along a rectilinear trajectory. We proceeded by analyzing the motion of a single surfer as a function of the forcing parameters, the surfer asymmetry, and its size (Fig. 1(d) and supplementary Figs. S1 and S2 in Ref. [61]). For a given surfer size and asymmetry, and at a fixed forcing frequency f, the surfer speed increases with the forcing acceleration γ. For a fixed acceleration amplitude, the speed decreases with frequency. In all cases, the surfers move significantly slower than the phase speed of their self-generated propagating waves.

In order to rationalize this dependence on the driving parameters, we consider the wave radiation stress generated by the surfer. The radiation stress S of surface waves may be defined as "the excess flow of momentum due to the presence of the waves" [62] and has the form $S = (3/4)\sigma A^2 k^2$ for capillary waves of amplitude A and wave number k. Note that this definition has units of force per length; nevertheless, we use the term stress or pressure to remain consistent with the prior literature [62]. Experimental measurements of the dependence of the surfer speed on its asymmetry show that the speed is maximized when the displacement of the center of mass relative to the in-plane geometric center is maximized, which corresponds to the highest difference in the equilibrium deformation of the liquid surface between stern and bow [inset of Fig. 1(d)]. The radiation stress generated by the surfer thus exhibits a fore-aft asymmetry: Waves of larger amplitude A_+ are generated at the stern, where the effective mass is larger, while waves of smaller amplitude A_- are generated at the bow. As a result, the surfer experiences a net propulsive force $F_p = (3/4)\sigma k^2 w(A_+^2 - A_-^2)$ via an asymmetric momentum flux, where w is the surfer width. An analogous propulsion mechanism via an asymmetric self-generated capillary wavefield was suggested for floating drops [47] and a waterbound honeybee [52] and recently demonstrated via direct wavefield measurement for a robotic version of the capillary surfer, the "SurferBot" [58]. We assume that the wave amplitudes $A_\pm$ are proportional to the bath forcing amplitude γ/f^2 and, using the capillary wave dispersion relation to relate k and f, we define a nondimensional propulsion force $F_p^* = F_p/(\sigma w)$ that thus scales as

$$F_p^* \sim \left(\frac{\rho}{\sigma}\right)^{2/3} \gamma^2 f^{-8/3}. \tag{1}$$

Figure 1(d) shows that the experimental speed measurements for a single surfer over a range of driving amplitudes and frequencies can be collapsed along a single curve when plotted as a function of this nondimensional propulsion force (see raw data in supplementary Fig. S1 [61]), confirming the hypothesis of wave radiation stress as the mechanism underlying surfer propulsion. Additionally, for small speeds, this curve follows a linear trend which suggests a corresponding linear (viscous) resistance. Recent work has demonstrated that for disks pinned atop a fluid interface at similar scales, the principal resistance to motion along the interface arises from the skin friction over the

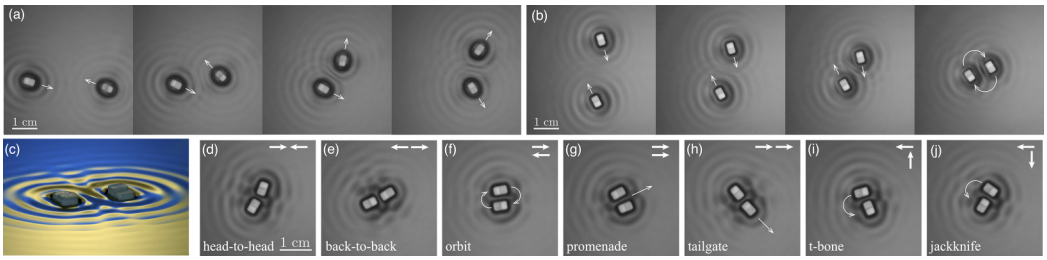

FIG. 2. Interaction of surfer pairs (see also supplementary video 2). (a) A collision yielding scattering. (b) A collision yielding a $n = 2$ orbit. (c) Oblique view of two orbiting surfers. [(d)–(j)] Bound modes observed in experiment with $n = 1$ for $f = 100$ Hz and $\gamma = 3.3$ g. (d) Head-to-head, (e) back-to-back, (f) orbit, (g) promenade, (h) tailgate, (i) t-bone, and (f) jackknife. In experiments, $L = 4.20 \pm 0.03$ mm, $w = 2.70 \pm 0.03$ mm, $a = L/2$.

wetted base of the disk [63]. Since the relevant viscous diffusion timescale ($t_\nu = H^2\rho/\eta$) in the present work is approximately 1 s, and the surfers typically move much less than a body length each second, we expect that a locally fully developed linear shear flow develops beneath the surfer leading to a linear drag law ($F_\nu \approx \eta U w L/H$). For higher speeds, deeper baths, less viscous working fluids, or partially immersed surfers, other nonlinear drag effects will likely become relevant.

Surfers may interact with each other through the propagating waves they generate on the fluid interface. Specifically, when two free surfers come within a few capillary wavelengths of each other, they deviate markedly from their rectilinear motion. This wave-mediated interaction has two possible outcomes. In a scattering process the surfers repel each other and ultimately recover rectilinear motions in new directions [Fig. 2(a)]. Alternatively, the surfers can enter a stable bound mode after a brief transient period [Fig. 2(b)]. In general, the outcome of the interaction depends on the initial condition of the surfers' relative motion. The number of bound modes varies with forcing frequency and amplitude. When the system was driven at $f = 100$ Hz and $\gamma = 3.3$ g (i.e., close to but below the Faraday instability threshold $\gamma_F = 3.80 \pm 0.05$ g) two surfers of equal size and speed with length $L = 4.20 \pm 0.03$ mm, width $w = 2.70 \pm 0.03$ mm, and $a = L/2$ exhibited the maximum number of bound modes. Variation of the experimental parameters, including liquid viscosity, generally resulted in a reduction of the number of observable modes. With these parameters, we observed up to seven qualitatively distinct bound modes [Figs. 2(d)–2(j) and supplementary video 2]: head-to-head (d), back-to-back (e), orbiting (f), promenade (g), tailgating (h), t-bone (i), and jackknife (j). In the head-to-head (back-to-back) mode the two surfer bows (sterns) face each other [Figs. 2(d) and 2(e)]. While these modes are static, the remaining five modes are dynamic. In the orbiting mode, the two surfers orbit around the system's center of mass [Fig. 2(f)]. In the promenade mode, they proceed side by side with constant speed along a rectilinear trajectory [Fig. 2(g)]. In the tailgating mode, the two surfers are aligned along their major axis, with the bow of one surfer pointing toward the stern of the other, and they move with constant speed along a rectilinear trajectory [Fig. 2(h)]. In the t-bone mode, the two major axes are perpendicular to each other and the bow of one surfer points toward the stern of the other, while they both execute a circular trajectory [Fig. 2(i)]. The jackknife mode has a similar configuration except the two sterns are close to each other [Fig. 2(j)]. Curiously, this rich catalog of bound modes shares many similarities with recent numerical predictions of pairwise bound modes for fully immersed two-sphere swimmers at intermediate Reynolds number [64] despite the apparently different fluid mechanisms mediating the interactions. In particular, the two-sphere swimmer recovers stable modes with similar arrangements to the following, back-to-back, promenade, and orbiting modes observed in the present interfacial system. In our system, bound modes can be obtained by either varying the initial conditions of a two-surfer impact or by varying the initial positions and orientations of two surfers manually positioned near one another. The back-to-back, tailgaiting and jackknife modes could not be realized in an impact event. Note that

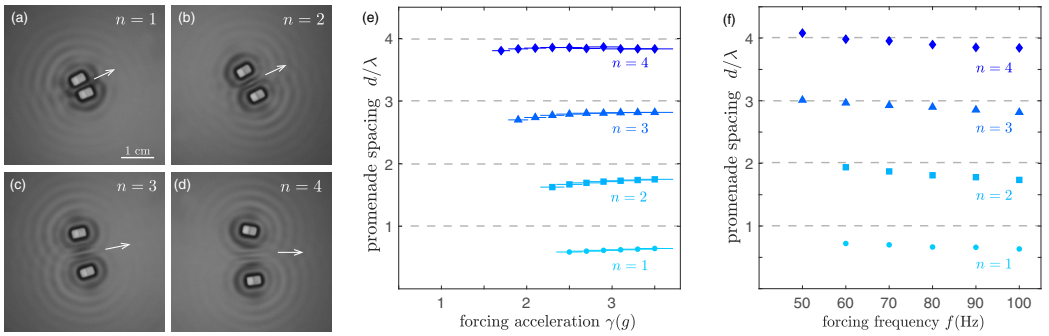

FIG. 3. Promenade modes. In (a)–(d), $\gamma = 3.3$ g and $f = 100$ Hz. (e) Dependence of the dimensionless intersurfer spacing d/λ on the forcing acceleration γ for fixed forcing frequency $f = 100$ Hz. (f) Dependence of d/λ on f just below the Faraday instability threshold. f ranges from 50–100 Hz in increments of 10 Hz, and the corresponding values of γ/g are 1.1, 1.5, 2.0, 2.3, 3.0, and 3.3. d is defined here as the distance between the surfers' nearest edges or specifically the distance between the centers of mass minus the surfer width w. $L = 4.20 \pm 0.03$ mm, $w = 2.70 \pm 0.03$ mm, and $a = L/2$.

should the vibration be eliminated, the surfers cease to propel and immediately collapse in towards each other under the influence of capillary attraction [65]. In each mode the two surfers exhibit discrete equilibrium spacings $d \approx n\lambda$ where $n = 1, 2, \ldots$. The maximum order $n_{\max}$ is different for each mode and depends on the properties of the liquid, vibration, and surfers. $n_{\max}$ and the individual surfer speeds for each mode are available in the Supplemental Material [61]. We focused on the promenade mode as in our experiments it exhibited the largest $n_{\max} = 4$ (Fig. 3). First, we fixed the forcing frequency and measured the promenade spacing for increasing forcing acceleration. The spacing d increases very slightly with forcing acceleration γ [Fig. 3(e)] but is significantly more sensitive to the forcing frequency f. The normalized spacing d/λ is approximately independent of f, showing that the equilibrium spacings are quantized by the capillary wavelength in the range of forcing frequencies explored [Fig. 3(f)]. The promenade speed increased with n but was always lower than the speed of a single surfer. As an individual surfer's waves are being continuously generated and propagating outward, the time-averaged wave slope experienced by a neighboring surfer is zero. However, due to its own synchronized vertical oscillation, the time-averaged lateral wave *force* is nonzero and exhibits an oscillatory spatial dependence, a mechanism identified in recent theoretical work [66] and expanded on in our companion theoretical paper [67].

Many-body experiments show that capillary surfers have potential as constituents of a novel active system (Fig. 4 and supplementary video 3). For instance, a many-body promenade mode [Fig. 4(a)] and a superorbiting state of eight surfers [Fig. 4(b)] have been observed in experiments.

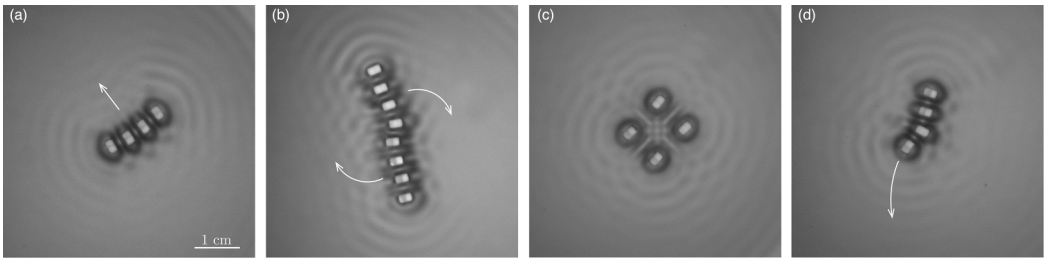

FIG. 4. Examples of collective behavior of surfers (supplementary video 3). (a) Promenade mode of four surfers. (b) Superorbiting mode of eight surfers. (c) Lattice mode of four surfers. (d) Composite mode of four surfers. Experimental parameters: $f = 100$ Hz, $\gamma = 3.3$ g, $L = 2.78 \pm 0.01$ mm, $w = 1.75 \pm 0.01$ mm, and $a = L/2$.

Multiple surfers can also arrange in static lattices [Fig. 4(c)] or exhibit exotic roto-translating bound states [Fig. 4(d)]. While there have been extensive studies on overdamped active systems [2], mediated by viscous hydrodynamic forces that decay monotonically with distance, a collection of surfers has the peculiar feature of being characterized by wave-mediated interactions, which results in long-range spatially oscillatory forces defined by alternating regions of attraction and repulsion. This feature is a consequence of fluid inertia and responsible for the multistability of a discrete set of interaction states, as documented here for the promenade mode (Fig. 3).

Collective behaviors at a fluid interface have been observed with camphor boats [68] and walking droplets [34] previously but only within a relatively narrow parameter space defined by the physical constraints of these systems. The two-surfer interaction landscape (Fig. 2) already far exceeds those documented for the aforementioned systems. Ultimately, the surfer system is a largely tunable and accessible experimental platform that has the potential to fill the gap between active systems at low and high Reynolds numbers: The surfers used in the present work self-propel at intermediate Reynolds number $\mathrm{Re} = \rho UL/\eta \sim O(1)$, where both fluid inertia and viscous forces are relevant. Recent reviews [25,26] underline the need for experimental platforms and theoretical frameworks to explore active systems in this intermediate regime, which has received far less attention than the purely viscous and inertial limits. It is anticipated that such systems could exhibit novel classes of self-organizing behaviors, such as soliton-like waves, shocklike phenomena, new flocking states (e.g., Fig. 4), and nonequilibrium phase transitions [25,26].

A.U.O. acknowledges support from the Simons Foundation (Collaboration Grant for Mathematicians Award No. 587006) and NSF DMS-2108839. G.P. acknowledges the CNRS Momentum program for its support. D.M.H. acknowledges support from the Office of Naval Research (ONR N00014-21-1-2816) and the Brown Undergraduate Teaching and Research Award. Additionally, the authors thank Professor Roberto Zenit for use of the conical rheometer.

[1] S. Ramaswamy, The mechanics and statistics of active matter, Annu. Rev. Condens. Matter Phys. **1**, 323 (2010).

[2] M. C. Marchetti, J.-F. Joanny, S. Ramaswamy, T. B. Liverpool, J. Prost, M. Rao, and R. A. Simha, Hydrodynamics of soft active matter, Rev. Mod. Phys. **85**, 1143 (2013).

[3] D. Saintillan and M. J. Shelley, Orientational Order and Instabilities in Suspensions of Self-Locomoting Rods, Phys. Rev. Lett. **99**, 058102 (2007).

[4] A. Sokolov and I. S. Aranson, Reduction of Viscosity in Suspension of Swimming Bacteria, Phys. Rev. Lett. **103**, 148101 (2009).

[5] T. Sanchez, D. T. N. Chen, S. J. DeCamp, M. Heymann, and Z. Dogic, Spontaneous motion in hierarchically assembled active matter, Nature (Lond.) **491**, 431 (2012).

[6] H. H. Wensink, J. Dunkel, S. Heidenreich, K. Drescher, R. E. Goldstein, H. Löwen, and J. M. Yeomans, Meso-scale turbulence in living fluids, Proc. Natl. Acad. Sci. USA **109**, 14308 (2012).

[7] J. Palacci, S. Sacanna, A. P. Steinberg, D. J. Pine, and P. M. Chaikin, Living crystals of light-activated colloidal surfers, Science **339**, 936 (2013).

[8] R. Golestanian, Collective Behavior of Thermally Active Colloids, Phys. Rev. Lett. **108**, 038303 (2012).

[9] A. P. Solon, J. Stenhammar, R. Wittkowski, M. Kardar, Y. Kafri, M. E. Cates, and J. Tailleur, Pressure and Phase Equilibria in Interacting Active Brownian Spheres, Phys. Rev. Lett. **114**, 198301 (2015).

[10] Q. Brosseau, F. B. Usabiaga, E. Lushi, Y. Wu, L. Ristroph, J. Zhang, M. Ward, and M. J. Shelley, Relating Rheotaxis and Hydrodynamic Actuation using Asymmetric Gold-Platinum Phoretic Rods, Phys. Rev. Lett. **123**, 178004 (2019).

[11] L. Huber, R. Suzuki, T. Krüger, E. Frey, and A. Bausch, Emergence of coexisting ordered states in active matter systems, Science **361**, 255 (2018).

[12] A. Doostmohammadi, J. Ignés-Mullol, J. M. Yeomans, and F. Sagués, Active nematics, Nat. Commun. **9**, 3246 (2018).
[13] V. Soni, E. S. Bililign, S. Magkiriadou, S. Sacanna, D. Bartolo, M. J. Shelley, and W. T. M. Irvine, The odd free surface flows of a colloidal chiral fluid, Nat. Phys. **15**, 1188 (2019).
[14] A. Bricard, J.-B. Caussin, N. Desreumaux, O. Dauchot, and D. Bartolo, Emergence of macroscopic directed motion in populations of motile colloids, Nature (Lond.) **503**, 95 (2013).
[15] M. Driscoll, B. Delmotte, M. Youssef, S. Sacanna, A. Donev, and P. Chaikin, Unstable fronts and motile structures formed by microrollers, Nat. Phys. **13**, 375 (2017).
[16] K. Yeo, E. Lushi, and P. M. Vlahovska, Collective Dynamics in a Binary Mixture of Hydrodynamically Coupled Microrotors, Phys. Rev. Lett. **114**, 188301 (2015).
[17] P. B. S. Lissaman and C. A. Shollenberger, Formation flight of birds, Science **168**, 1003 (1970).
[18] D. Weihs, Hydromechanics of fish schooling, Nature (Lond.) **241**, 290 (1973).
[19] A. Attanasi, A. Cavagna, L. D. Castello, I. Giardina, T. S. Grigera, A. Jelić, S. Melillo, L. Parisi, O. Pohl, E. Shen, and M. Viale, Information transfer and behavioural inertia in starling flocks, Nat. Phys. **10**, 691 (2014).
[20] A. D. Becker, H. Masoud, J. W. Newbolt, M. Shelley, and L. Ristroph, Hydrodynamic schooling of flapping swimmers, Nat. Commun. **6**, 8514 (2015).
[21] A. U. Oza, L. Ristroph, and M. J. Shelley, Lattices of Hydrodynamically Interacting Flapping Swimmers, Phys. Rev. X **9**, 041024 (2019).
[22] C. Scholz, S. Jahanshahi, A. Ldov, and H. Löwen, Inertial delay of self-propelled particles, Nat. Commun. **9**, 5156 (2018).
[23] S. Mandal, B. Liebchen, and H. Löwen, Motility-Induced Temperature Difference in Coexisting Phases, Phys. Rev. Lett. **123**, 228001 (2019).
[24] D. Banerjee, A. Souslov, A. G. Abanov, and V. Vitelli, Odd viscosity in chiral active fluids, Nat. Commun. **8**, 1573 (2017).
[25] D. Klotsa, As above, so below, and also in between: Mesoscale active matter in fluids, Soft Matter **15**, 8946 (2019).
[26] C. Bechinger, R. Di Leonardo, H. Löwen, C. Reichhardt, G. Volpe, and G. Volpe, Active particles in complex and crowded environments, Rev. Mod. Phys. **88**, 045006 (2016).
[27] S. Dorbolo, D. Volfson, L. Tsimring, and A. Kudrolli, Dynamics of a Bouncing Dimer, Phys. Rev. Lett. **95**, 044101 (2005).
[28] Y. Couder, S. Protiere, E. Fort, and A. Boudaoud, Walking and orbiting droplets, Nature (Lond.) **437**, 208 (2005).
[29] V. Narayan, S. Ramaswamy, and N. Menon, Long-lived giant number fluctuations in a swarming granular nematic, Science **317**, 105 (2007).
[30] I. S. Aranson, D. Volfson, and L. S. Tsimring, Swirling motion in a system of vibrated elongated particles, Phys. Rev. E **75**, 051301 (2007).
[31] A. Kudrolli, G. Lumay, D. Volfson, and L. S. Tsimring, Swarming and Swirling in Self-Propelled Polar Granular Rods, Phys. Rev. Lett. **100**, 058001 (2008).
[32] J. Deseigne, O. Dauchot, and H. Chaté, Collective Motion of Vibrated Polar Disks, Phys. Rev. Lett. **105**, 098001 (2010).
[33] M. Workamp, G. Ramirez, K. E. Daniels, and J. A. Dijksman, Symmetry-reversals in chiral active matter, Soft Matter **14**, 5572 (2018).
[34] P. J. Sáenz, G. Pucci, S. E. Turton, A. Goujon, R. R. Rosales, J. Dunkel, and J. W. M. Bush, Emergent order in hydrodynamic spin lattices, Nature (Lond.) **596**, 58 (2021).
[35] L. Giomi, N. Hawley-Weld, and L. Mahadevan, Swarming, swirling and stasis in sequestered bristle-bots, Proc. R. Soc. A **469**, 20120637 (2013).
[36] A. Deblais, T. Barois, T. Guerin, P.-H. Delville, R. Vaudaine, J. S. Lintuvuori, J.-F. Boudet, J.-C. Baret, and H. Kellay, Boundaries Control Collective Dynamics of Inertial Self-Propelled Robots, Phys. Rev. Lett. **120**, 188002 (2018).
[37] D. Yamada, T. Hondou, and M. Sano, Coherent dynamics of an asymmetric particle in a vertically vibrating bed, Phys. Rev. E **67**, 040301(R) (2003).

[38] N. Koumakis, A. Gnoli, C. Maggi, A. Puglisi, and R. Di Leonardo, Mechanism of self-propulsion in 3D-printed active granular particles, New J. Phys. **18**, 113046 (2016).
[39] H. Chaté, Dry aligning dilute active matter, Annu. Rev. Condens. Matter Phys. **11**, 189 (2019).
[40] J. W. M. Bush and D. L. Hu, Walking on water: Biolocomotion at the interface, Annu. Rev. Fluid Mech. **38**, 339 (2006).
[41] M. Nagayama, S. Nakata, Y. Doi, and Y. Hayashima, A theoretical and experimental study on the unidirectional motion of a camphor disk, Phys. D: Nonlin. Phenom. **194**, 151 (2004).
[42] A. Snezhko, M. Belkin, I. S. Aranson, and W.-K. Kwok, Self-Assembled Magnetic Surface Swimmers, Phys. Rev. Lett. **102**, 118103 (2009).
[43] S. K. Chung, K. Ryu, and S. K. Cho, Electrowetting propulsion of water-floating objects, Appl. Phys. Lett. **95**, 014107 (2009).
[44] G. Grosjean, G. Lagubeau, A. Darras, M. Hubert, G. Lumay, and N. Vandewalle, Remote control of self-assembled microswimmers, Sci. Rep. **5**, 16035 (2015).
[45] J. Yang, M. Davoodianidalik, H. Xia, H. Punzmann, M. Shats, and N. Francois, Passive propulsion in turbulent flows, Phys. Rev. Fluids **4**, 104608 (2019).
[46] G. Pucci, E. Fort, M. Ben Amar, and Y. Couder, Mutual Adaptation of a Faraday Instability Pattern with Its Flexible Boundaries in Floating Fluid Drops, Phys. Rev. Lett. **106**, 024503 (2011).
[47] G. Pucci, Faraday instability in floating drops out of equilibrium: Motion and self-propulsion from wave radiation stress, Int. J. Non-Lin. Mech. **75**, 107 (2015).
[48] H. Ebata and M. Sano, Swimming droplets driven by a surface wave, Sci. Rep. **5**, 8546 (2015).
[49] Y. Chen, N. Doshi, B. Goldberg, H. Wang, and R. J. Wood, Controllable water surface to underwater transition through electrowetting in a hybrid terrestrial-aquatic microrobot, Nat. Commun. **9**, 2495 (2018).
[50] J. W. M. Bush and A. U. Oza, Hydrodynamic quantum analogs, Rep. Prog. Phys. **84**, 017001 (2021).
[51] T. Steinmann, M. Arutkin, P. Cochard, E. Raphaël, J. Casas, and M. Benzaquen, Unsteady wave pattern generation by water striders, J. Fluid Mech. **848**, 370 (2018).
[52] C. Roh and M. Gharib, Honeybees use their wings for water surface locomotion, Proc. Natl. Acad. Sci. USA **116**, 24446 (2019).
[53] R. S. Wilcox, Communication by surface waves, J. Comp. Physiol. **80**, 255 (1972).
[54] H. Bleckmann, M. Borchardt, P. Horn, and P. Görner, Stimulus discrimination and wave source localization in fishing spiders (*Dolomedes triton and D. okefinokensis*), J. Comp. Physiol. A **174**, 305 (1994).
[55] P. Wright and J. Saylor, Patterning of particulate films using Faraday waves, Rev. Sci. Instrum. **74**, 4063 (2003).
[56] G. Falkovich, A. Weinberg, P. Denissenko, and S. Lukaschuk, Floater clustering in a standing wave, Nature (Lond.) **435**, 1045 (2005).
[57] H. Punzmann, N. Francois, H. Xia, G. Falkovich, and M. Shats, Generation and reversal of surface flows by propagating waves, Nat. Phys. **10**, 658 (2014).
[58] E. Rhee, R. Hunt, S. J. Thomson, and D. M. Harris, SurferBot: a wave-propelled aquatic vibrobot, Bioinspiration Biomim. **17**, 055001 (2022).
[59] M. Faraday, On a peculiar class of acoustical figures; and on certain forms assumed by groups of particles upon vibrating elastic surfaces, Philos. Trans. R. Soc. Lond. **121**, 299 (1831).
[60] C. Sanlı, D. Lohse, and D. van der Meer, From antinode clusters to node clusters: the concentration-dependent transition of floaters on a standing Faraday wave, Phys. Rev. E **89**, 053011 (2014).
[61] See Supplemental Material at http://link.aps.org/supplemental/10.1103/PhysRevFluids.8.L112001 for supplementary figures and videos, and additional details on experimental methods.
[62] M. S. Longuet-Higgins and R. W. Stewart, Radiation stresses in water waves; a physical discussion, with applications, Deep-Sea Res. **11**, 529 (1964).
[63] G. Pucci, I. Ho, and D. M. Harris, Friction on water sliders, Sci. Rep. **9**, 4095 (2019).
[64] T. Dombrowski, H. Nguyen, and D. Klotsa, Pairwise interactions between model swimmers at intermediate Reynolds numbers, Phys. Rev. Fluids **7**, 074401 (2022).
[65] I. Ho, G. Pucci, and D. M. Harris, Direct Measurement of Capillary Attraction between Floating Disks, Phys. Rev. Lett. **123**, 254502 (2019).

[66] M. De Corato and V. Garbin, Capillary interactions between dynamically forced particles adsorbed at a planar interface and on a bubble, J. Fluid Mech. **847**, 71 (2018).
[67] A. U. Oza, G. Pucci, I. Ho, and D. M. Harris, following paper, Theoretical modeling of capillary surfer interactions on a vibrating fluid bath, Phys. Rev. Fluids **8**, 114001 (2023).
[68] N. J. Suematsu, S. Nakata, A. Awazu, and H. Nishimori, Collective behavior of inanimate boats, Phys. Rev. E **81**, 056210 (2010).

Supplemental Material: Capillary surfers: wave-driven particles at a vibrating fluid interface

Ian Ho[1,†], Giuseppe Pucci[1,2,†], Anand U. Oza[3] & Daniel M. Harris[1,*]

[1] School of Engineering, Brown University, 184 Hope Street, Providence, Rhode Island 02912, USA

[2] Univ Rennes, CNRS, IPR (Institut de Physique de Rennes)—UMR 6251, F-35000 Rennes, France

[3] Department of Mathematical Sciences & Center for Applied Mathematics and Statistics, New Jersey Institute of Technology, Newark, New Jersey 07102, USA

*corresponding author, †co-first author

I. EXPERIMENTAL METHODS

A. Liquid bath

A bath of diameter 10 cm was filled with a glycerol-water mixture. In order to precisely infer the volume fraction of glycerol, we measured the mixture density $\rho = 1.1755 \pm 0.0001$ g/cm^3 at $T = 21.7$ °C with a densitometer (DM 35 Basic, Anton Paar). Using an empirical formula [1] the glycerol volume fraction was determined to be 63.2%. The dynamic viscosity $\eta = 0.0192 \pm 0.0002$ Pa·s was measured at $T = 22.0$ °C using a conical rheometer (ARES-G2, TA Instruments), a result that is in close agreement with the viscosity $\eta = 0.0184$ Pa·s obtained at the same temperature from an empirical formula [2].

All experiments were conducted at the temperature $T = 21.5 \pm 0.5$ °C, at which $\rho = 1.1756 \pm 0.0003$ g/cm^3 and $\eta = 0.0197 \pm 0.0005$ Pa·s, where uncertainties are due to temperature fluctuations and estimated from empirical formulae [1, 2]. The surface tension $\sigma = 66.4 \pm 0.5$ mN/m was measured at $T = 21.5$ °C via a pendant drop method [3]. A graduated cylinder with resolution 1 mL was used to measure and pour 45 mL of liquid into the bath. The resulting depth of the bath was $H = 5.73 \pm 0.06$ mm. The Faraday instability threshold γ_F of the vibrated bath was measured before, in between, and after sets of experiments in order to ensure that the physical properties of the liquid remained unchanged, and always ranged in the interval $\gamma_F = 3.75$–3.85 g for the forcing frequency $f = 100$ Hz.

B. Vibration setup

The bath container was made of acrylic and directly mounted on an electrodynamic shaker (The Modal Shop, 2025E) connected to an amplifier (The Modal Shop, 2100E21). Two accelerometers (PCB Piezoelectronics, 352C65) were attached at diametrically opposed ends of the container and their signals were acquired by a computer through a data acquisition device (National Instruments, USE-6343). The reported acceleration was the mean of the measurements of the accelerometers. A closed feedback loop was used to maintain the mean acceleration at a specified target value. The acceleration difference between the accelerometers was also recorded at each frequency. The shaker was mounted on a isolated optical bench (Thorlabs, SDA75120) to reduce the influence of external vibrations. A monochrome USB camera (Allied Vision, Mako) with a macro lens for video acquisition was mounted above the bath and normal to its surface. In order to increase the contrast of the video recordings, the bath's base was constructed of a black acrylic plate. The system was placed inside an acrylic box to isolate the bath from ambient air currents and contaminants.

C. Visualization

Tracking was performed with the surfers appearing as white objects on a dark bath on the recordings of a camera placed vertically above the bath. The wave field was visualized using a semi-transparent mirror placed at 45 degrees relative to the vertical, and directly above the fluid bath. A light source with diffuser was directed horizontally toward the mirror. A black backdrop was placed behind the mirror to minimize exterior sources of light, and the camera was placed vertically above the mirror. An in-sync strobing effect was obtained with the camera and triggered at a frequency that was an integer divisor of f. Out-of-sync videos were recorded with the camera frame rate slightly detuned from f. High speed videos were recorded with a Phantom Miro R311 color high-speed camera with oblique orientation with respect to the bath using a reflection technique to visualize the waves [4].

D. Preliminary tests

The speed of 15 surfers with $L = 4.2$ mm, $w = 2.7$ mm and asymmetry parameter $a = L/2$ (Fig. 1(b) in the manuscript) was measured for $\gamma = 3.5$ g and $f = 100$ Hz. The mean speed was $U = 2.27$ mm/s with standard deviation 0.25 mm/s. Among the 15 surfers, 6 were selected for the experiments as those exhibiting the straightest trajectories. Imperfections in the pinning of the contact line were observed to lead to curved trajectories.

E. Experimental procedures

Prior to each experiment, the liquid container was cleaned with ethanol, rinsed with deionized water and dried with clean compressed air. In order to avoid the effects of wave reflection or waves due to the oscillating meniscus at the border of the bath, data were only recorded when the surfers were within 26.5 mm of the bath center, where the surfer velocity was measured to be statistically independent of its proximity to the border. During single-surfer speed measurements, the fluid bath was changed for every 3 surfers tested. A linear least-squares fit was used to calculate the time-averaged speed of the surfer from the distance traveled by the surfer as a function of time. At $f = 100$ Hz the error on the time-averaged speed ranged from 0.0001–0.001 mm/s, with a 95% confidence bound for a single surfer. The standard deviation among 6 surfers ranged from 0.01–0.1 mm/s.

The interaction modes of surfer pairs (Fig.2(d–j) in the manuscript) were explored with 6 pairs, chosen among the 6 surfers according to the best similarity in propulsion speed. Here the fluid bath was changed and refreshed for every new pair. For the promenade spacing measurements at $f = 100$ Hz (Fig. 3(e) in the manuscript), the standard deviation of the spacing among pairs of surfers ranged from 0.01–0.1 mm.

For the inset of Fig. 1(d) in the manuscript, the position of the surfer's center of mass was varied by varying the length of the PTFE upper layer in a surfer with $L = 6.44 \pm 0.02$ mm and $w = 4.13 \pm 0.02$ mm. These surfers were slightly larger than those used elsewhere in the paper in order to ease the manufacturing process. Five different positions of the center of mass were explored and six surfers were used per position.

Surfers with five different sizes were used to investigate the effect of magnification. Six surfers per size were used. Each surfer was a scaled-up version of a sample surfer (so that the width, length and corner radius of curvature were magnified by a constant) but with the thicknesses kept constant. Each surfer had asymmetry parameter $a = L/2$. Here the fluid bath was changed every time the experiments on two surfers were completed. These results are reported in Fig. S2.

F. Uncertainties and error propagation

The uncertainty on the surfer non-dimensional propulsive force scaling was calculated by substituting the formula for the wavenumber of capillary waves in the deep-water limit, $k = (\rho\omega^2/\sigma)^{1/3}$, and $\omega = 2\pi f$ into

Eq. 1 (Main Text) and computing the square root of the variance formula for independent variables:

$$\Delta F_p^* = \sqrt{\left(\frac{\partial F_p^*}{\partial \sigma}\right)^2 \Delta\sigma^2 + \left(\frac{\partial F_p^*}{\partial \gamma}\right)^2 \Delta\gamma^2 + \left(\frac{\partial F_p^*}{\partial f}\right)^2 \Delta f^2 + \left(\frac{\partial F_p^*}{\partial \rho}\right)^2 \Delta\rho^2}, \tag{1}$$

where $\Delta\sigma = 0.5$ mN/m, $\Delta f = 0.1$ Hz, and $\Delta\rho = 0.0003$ g/cm^3. The uncertainty in the forcing acceleration $\Delta\gamma/\gamma = 0.01$–$0.06$ was measured in the range of frequency 40–100 Hz as the largest discrepancy between the measurements of the two accelerometers. The horizontal error bars in Fig. 1(d) in the manuscript represent the resulting uncertainty ΔF_p^*.

II. SUPPLEMENTARY FIGURES AND TABLES

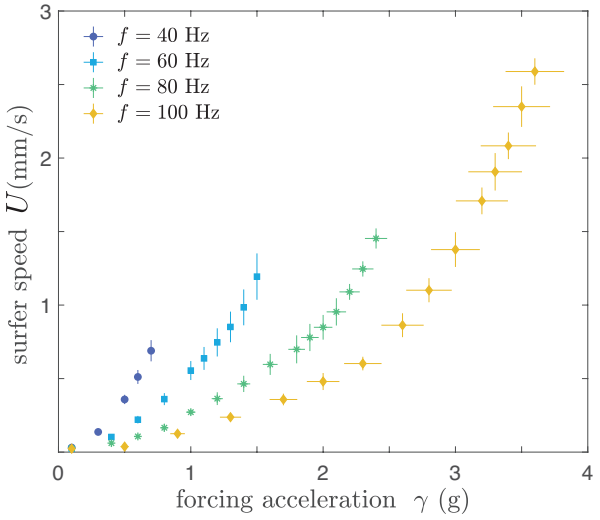

Supplementary Figure S1. Dependence of surfer speed U on forcing frequency f and forcing amplitude γ. $L = 4.20 \pm 0.03$ mm, $w = 2.70 \pm 0.03$ mm, $a = L/2$. The height of the surfer's stern and bow were $h_+ = 1.22$ mm and $h_- = 0.82$ mm, respectively.

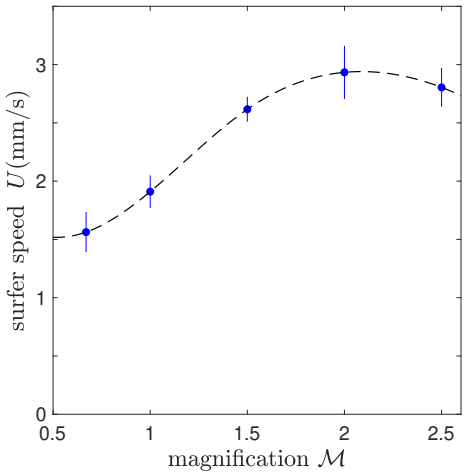

Supplementary Figure S2. Dependence of surfer speed on its magnification for $a = L/2$, $\gamma = 3.3$ g, and $f = 100$ Hz. Each surfer was a scaled-up version of a sample surfer (so that the width, length and corner radius of curvature were magnified by a constant) but with the overall thickness kept constant. $\mathcal{M} = 1$ corresponds to $L = 4.20 \pm 0.03$ mm and $w = 2.70 \pm 0.03$ mm. The height of the surfer's stern and bow were $h_+ = 1.22$ mm and $h_- = 0.82$ mm in all cases.

n	**orbit**	**promenade**	**tailgate**	**t-bone**	**jackknife**
1	2.1±0.2	1.5 ± 0.2	1.7 ± 0.2	2.2 ± 0.1 0.7 ± 0.3	2.9 ± 0.2 1.8 ± 0.1
2	2.1±0.1	1.6 ± 0.2			2.3 ± 0.2 1.5 ± 0.2
3		1.8 ± 0.2			
4		1.9 ± 0.2			

Supplementary Table S1. Speed (mm/s) of surfers in the dynamic bound modes observed. n denotes mode order and only stable mode orders are reported. Note that in the t-bone and jackknife modes the two surfers have different speeds. Uncertainties correspond to one standard deviation on the speed of six pairs of surfers. $f = 100$ Hz, $\gamma = 3.3$ g, $L = 4.20 \pm 0.03$ mm, $w = 2.70 \pm 0.03$ mm, $a = L/2$. The free, single-surfer speed with the same parameters is 2.0 ± 0.1 mm/s.

III. SUPPLEMENTARY VIDEOS

Supplementary Video 1

Experimental observation of single surfer propulsion. Details and parameters are provided in the video.

Supplementary Video 2

Two surfer interaction modes obtained in experiments. Details and parameters are provided in the video.

Supplementary Video 3

Sample multiple surfer interaction modes observed in experiments. Details and parameters are provided in the video.

---

[1] A. Volk and C. J. Kähler, "Density model for aqueous glycerol solutions," *Exp. Fluids*, vol. 59, no. 5, p. 75, 2018.

[2] N.-S. Cheng, "Formula for the viscosity of a glycerol-water mixture," *Ind. Eng. Chem. Res.*, vol. 47, no. 9, pp. 3285–3288, 2008.

[3] A. Daerr and A. Mogne, "Pendent_drop: an ImageJ plugin to measure the surface tension from an image of a pendent drop," *J. Open Res. Softw.*, vol. 4, no. 1, 2016.

[4] D. M. Harris, J. Quintela, V. Prost, P.-T. Brun, and J. W. M. Bush, "Visualization of hydrodynamic pilot-wave phenomena," *J. Vis.*, vol. 20, no. 1, pp. 13–15, 2017.